

UCSF

UC San Francisco Electronic Theses and Dissertations

Title

Statistical Shape Analysis on MRI

Permalink

<https://escholarship.org/uc/item/4cp8t6x4>

Author

Sadeghi, Roksana

Publication Date

2015

Peer reviewed|Thesis/dissertation

Statistical Shape Analysis on MRI

by

Roksana Sadeghi

THESIS

Submitted in partial satisfaction of the requirements for the degree of

MASTER OF SCIENCE

in

Biomedical Imaging

in the

GRADUATE DIVISION

Copyright 2015
by
Roksana Sadeghi

Acknowledgments

Firstly, I would like to express my sincere gratitude to my advisor Prof. Norbert Schuff for the continuous support of my M.Sc study and related research, for his patience, motivation, and immense knowledge. His guidance helped me in all the time of research and writing of this thesis. I could not have imagined having a better advisor and mentor for my study.

Besides my advisor, I would like to thank the rest of my thesis committee: Prof. David Saloner, Prof. Duygu Tosun, and Prof. Dieter Meyerhoff, for their insightful comments and encouragement, but also for the hard question which incited me to widen my research from various perspectives.

My sincere thanks also goes to Dr. Thanh Le, Dr. Nicolas Pannetier and Katherine Wu, who provided me an opportunity to join their team as intern, and who gave access to the laboratory and research facilities. Without their precious support it would not have been possible to conduct this research.

Last but not the least, I would like to thank my family: my parents and my brother and sister for supporting me spiritually throughout writing this thesis and my life in general.

Statistical Shape analysis on MRI

Roksana Sadeghi

Abstract

Medical imaging including magnetic resonance imaging (MRI) has become a major source of information for making clinical decisions, specifically based on static and dynamic shape variations of organs and moving structures respectively. Most conventional algorithms for shape extraction from images rely on deterministic modeling that offers no quantification for confidence of the extracted shapes. In this thesis a probabilistic approach for shape extraction is tested that provides a degree of confidence in extracted shapes. The degree of confidence create the important information in clinical decisions. This novel method, termed probabilistic Bayesian shape analysis introduced by Le.T and Schuff.N in [1], utilizes Curvelet transformation and Hidden Markov model simultaneously to detect probabilistic distributions of shape contours. In addition, this thesis, aims to effectively summarize probabilistic shape features in terms of information theoretic measures, such as the entropy (E) and statistical complexity (SC). The approach was initially demonstrated on well-defined hand gestures. To show the clinical potential of probabilistic shape feature extraction, the novel method was tested on tongue shape variations during pronunciation of vowels. Probabilistic shape analysis of tongue movement during vowel pronunciations mapped on MRI was performed on 5 subjects [1 woman, 4 men, age range 25-58], who speak English. MRI consisted of a Fast Low Angle Shot sequence [2]. All subjects were asked to sequentially pronounce the vowels [u:], [i:], [a:], [ae:], [e:], [o:], each for approximately 7 seconds, while having the fast MRI scan of the tongue. A probabilistic contour of tongue shape was extracted from each MRI frame ($total = 210$) and its features were summarized in terms of E and SC. Variations in E and SC as a function of vowel were then tested using univariate linear mixed effects regression. In addition, a multivariate linear mixed effects regression based on Monte Carlo sampling was used to test variations in E and SC simultaneously. First, the analysis showed that the novel method significantly captures variations in tongue shapes compared to repeated MRI variations. Second, the analysis demonstrated that entropy of the tongue extracted consistent shapes for the vowels [u:], [ae:], and [o:] across subjects, and for SC consistent features were found for [u:], [ae:], [a:] and [o:]. Moreover, using E and SC together capture consistent features for the vowels [a:], [e:], [i:] and [u:] across subjects. In conclusion, this thesis illustrated that the probabilistic shape model captures tongue shapes associated with vowel pronunciation. The new method is of potential interest to clinical studies of tongue disorders and function, including speech therapy, assessment of tongue surgery and assessment of functionality of the tongue. Beyond the tongue, the novel probabilistic approach has potentially wide clinical applications in almost any medical field that uses imaging. Examples of applications for the importance of contour extraction and shape detection include the delineation of almost any organ, such as the shape of kidneys and liver, the changing shapes of tendons in joints during movement, the tracking of change in structure of the beating heart and the shape of a tumor, specifically in the brain.

Contents

1	Introduction	1
2	Background	3
2.1	Conventional Shape Representation Algorithms	3
2.2	Shape Constraints	3
2.3	Shape Quantification	4
2.4	Probabilistic Shape Modeling	5
3	Theory	6
3.1	Sparse Image Representation	6
3.1.1	Curvelet Transformation	6
3.2	Markov Chain and Hidden Markov Model	8
3.2.1	Markov Chain Model	8
3.2.2	Hidden Markov Model (HMM)	8
3.2.3	Hidden Semi Markov Model (HSMM)	9
3.2.4	HSMM training	10
3.3	Information Theoretic Measures	10
3.3.1	Entropy	11
3.3.2	Statistical Complexity	11
3.3.3	Jensen-Shannon Divergence	11
4	Method	12
4.1	Subjects and Study Protocol	12
4.2	MRI Acquisition	12
4.3	Preprocessing	13
4.4	Bayesian Contour Extraction	13
4.4.1	Curvelet Representation	13
4.4.2	Defining Intensity of Contour Representation	14
4.4.3	Deriving the probability of contour progression	14
4.4.4	Selecting Best Progression Point	14
4.4.5	Bias Reduction	15
4.5	Feature Extraction	16
4.6	Quantification of Features	17
4.7	Computational language method	17
4.8	Statistics	17

5	Initial Test	19
6	Main Results - Tongue Shapes	21
7	Discussion and Conclusion	26

List of Figures

2.1	H and U simulated shapes and their detected contours with Basis Snake (BS), Balloon Forced Snake (BFS), Gradient Vector Flow (GVF) and Greedy Snake (GDS) algorithms [1].	4
2.2	H and U simulated shapes and their detected contours using the probabilistic shape model [1]	5
3.1	Curvelets in Fourier frequency (left) and spatial domain (right) [3].	7
3.2	Eight connected chain coding to achieve 8-angular resolution [1].	8
4.1	Flow chart of Bayesian Contour extraction modeling.	13
5.1	Different hand gestures numbering one to five, respectively.	19
5.2	The green lines shows extracted contours using the novel probabilistic shape model.	19
5.3	Plot of SC versus E for different hand gestures. Colors indicate the various hand gestures shown in figure 5.1. Note, the clustering in SC and E for most hand shapes.	20
6.1	Representative MRI data from a subject pronouncing 6 vowels. The images have been acquired with MRI Skyra system with 32 channel head coil and the Flash sequence. The important parameters of the sequence can be found in the images. The images in the first row corresponds to vowels [u:] and [i:], second row [a:] and [ae:] and third row [e:] and [o:], respectively.	21
6.2	Preprocessed images of the same subject as shown in figure 6.1 while pronouncing 6 vowels. The images in the first row corresponds to vowels [u:], [i:] and [a:] and second row [ae:], [e:] and [o:], respectively.	22
6.3	Contours extraction of the same subject pronouncing different vowels.	22
6.4	Different subjects pronouncing [i:] under the MR System.	23
6.5	Plot of SC versus E in 5 subjects	24

List of Tables

6.1	Univariate analysis of E and SC separately. This table contains p-values of variations from different vowels as well as different frames from univariate mixed effect model considering E and SC. Note, the one with * significantly detected with the corresponding model	25
6.2	Multivariate analysis of E and SC together. This table contains p-values of variations from different vowels as well as different frames from multivariate mixed model considering both E and SC. Note, the one with * significantly detected with the model	25

Chapter 1

Introduction

Medical imaging including magnetic resonance imaging (MRI), has become a major source of information for making informed clinical decisions, such as diagnoses, localizing organs pathology, planning surgeries and evaluating medical and surgical interventions. Especially anatomical features like location, shape, and size of organs or lesions often provide important clinical impressions about a medical condition. Humans can visually extract anatomical features to a certain degree by using expert knowledge. However, this approach is potentially influenced by reader bias. Additionally, for large number of images, i.e. in dynamic imaging, human reading is also ineffective and costly. With improving computer power, computational solutions to extract image features automatically have become increasingly attractive in clinical practice. These computational solutions generally rely on image contours that imply boundaries of anatomical structures. A variety of algorithms have been developed over the years to capture image contours of anatomical structures and to further facilitate quantitative measurements, such as volume, thickness and shapes on these structures. However, a major problem in this field is the precision in detecting contours in the presence of noise. The overarching goal of this thesis is to develop a computational framework that improves precision in contour detection and representation of anatomical structures in medical imaging.

Algorithms for extracting contours fall roughly into two fundamentally different classes: one class treats contours deterministically by establishing discrete landmark points along the contours; the other treats contours probabilistically by allowing a degree of uncertainty. In the deterministic approach it is assumed that the entire measurement process is known beforehand, that is, there are no errors by chance. Accordingly, deterministic contour evaluations usually rely on models that separate contour information, i.e. image contrast, from noise. On the contrary, in the probabilistic approach the element of chance is involved. Contrast variations are considered to be probabilistic, typically resulting from a hidden random process that the approach attempts to characterize. Contours are then derived from the maximum likelihood of their respective probability distributions given the contrast variations. Furthermore, a probabilistic approach offers the advantage that established rules of information theory can be applied to quantify the degree of confidence in the contour measurements. This thesis focuses on a novel probabilistic formalism for extraction contours and quantifying shapes.

Aside from developing a computational framework for probabilistic shapes, this thesis also

addresses the challenge to effectively summarize features of probabilistic shapes. A conventional and also straightforward summary metric for quantifying shape features is to take mean value and standard deviation of a set of contours. However, this method is very simplistic and only provides a global measure of shape without ability to capture potentially local shape variations. More sophisticated and popular methods for summarizing features are Principal Component Analysis (PCA) [4] and Fractal feature analysis [5]. PCA is a statistical procedure to bring out strong pattern in a dataset, called the principal components, based on variations. The largest principal components can be used to quantify some degree of the complexity in shapes. Fractal analysis allows assessing the characteristics of shapes in terms of complex patterns that are self-similar across different scales, so called fractals [5]. However, a fundamental limitation of both PCA and Fractal analysis is that they only operate on discrete input data that unlike probabilistic inputs - do not permit a degree of uncertainty. PCA is also limited in the way it transforms possibly correlated input variables into a set of linearly uncorrelated output variables while potentially nonlinear correlations are ignored. A critical limitation of fractal analysis is that the fractals are determined empirically and are not necessarily generalizable. To overcome the limitations of both PCA and Fractal analysis, this thesis utilized SC, a recently developed formalism for analyzing medical imaging data proposed by Young and Schuff in [6] to quantify probabilistic shape features.

The clinical importance of developing improved methods for shape measurements is that many diseases lead to deformations of affected organs and development of tumors or tissue lesions that can be visualized with medical imaging, e.g. using MRI. Similarly, dynamic imaging of shape changes is also increasingly being used in clinics to evaluate proper function of moving body parts and organs, such as joints and the heart. To demonstrate the clinical utility of the new probabilistic shape formalism in this thesis, variations in the shape of tongue during speech generation have been studied. Specifically, the degree to which the new probabilistic shape formalism captures consistent tongue shapes for vowel pronunciations has successfully been tested on normal human subjects. The new method should be of interest to clinical studies of tongue disorders and function, including speech therapy, assessment of tongue surgery and assessment of functionality of the tongue [7], [8]. Beyond the tongue, the novel probabilistic approach has potentially wide clinical applications in almost any medical field that employs imaging. Examples of potential applications include the delineation of almost any organ, such as the shape of kidneys and liver, the changing shapes of tendons in joints during movement, the tracking of change in structure of beating heart, and the shape of a tumor, specifically in the brain.

To summarize, the goal of this study is to implement a probabilistic approach to identify contours in images of anatomical shapes and to introduce a novel metric for quantifying shape variations based on information theory. As a test, a shape analysis of serial MRI data that maps tongue movement during vowel generation is presented.

Chapter 2

Background

2.1 Conventional Shape Representation Algorithms

In bio-medical imaging, analysis of static and dynamic anatomical morphology plays a central role for assessing abnormalities and diseases. Several methods for shape representation have been proposed over the years. Arguably the most popular and commonly used methodology so far has been deformable active contour models, termed Snakes [9].

An initial algorithm of Snakes, termed Basis Snake, has been introduced by Kass et al in 1988 [9]. This method starts with initial landmarks of shape boundaries and helps these landmarks to move toward ideal positions using energy minimization algorithms, which generally utilize intensity similarity for optimization. However, this approach requires images with high contrast and high signal to noise ratio to obtain robust contour estimates. In addition, the boundaries in Basis Snake highly depend on initial landmarks. The Balloon Force Snake [10] has been developed to address some of these drawbacks. Balloon Force Snake uses intensity gradients rather than direct intensities as energy minimization. This causes landmarks to move faster together toward the ideal shape boundaries driven by a global so-called internal pressure, which also results in lower sensitivity to initial conditions. However, contours can easily diverge from boundaries in Balloon Force Snake if the boundary energy, i.e. the gradient slope, is too small in comparison to the internal pressure [1]. To overcome this issue, the Greedy Snake [11] and Gradient Vector Flow [12] algorithms have been developed, in which the impact of the global pressure force is relaxed and each landmark is allowed to move through the boundaries separately. However, these algorithms still have a problem in absence of any pressure when no clear direction for landmark movement can be derived.

In summary, Snakes algorithms have fundamental limitations and are very sensitive to noise. For an illustration of the problems with Snakes, figure 2.1 shows contours based on various Snakes algorithms for U and H shaped objects that were obviously not always successful, despite high image contrast.

2.2 Shape Constraints

The performance of contour detection can often be improved by incorporating prior knowledge about the physical object features. An example of prior knowledge in medical imaging is

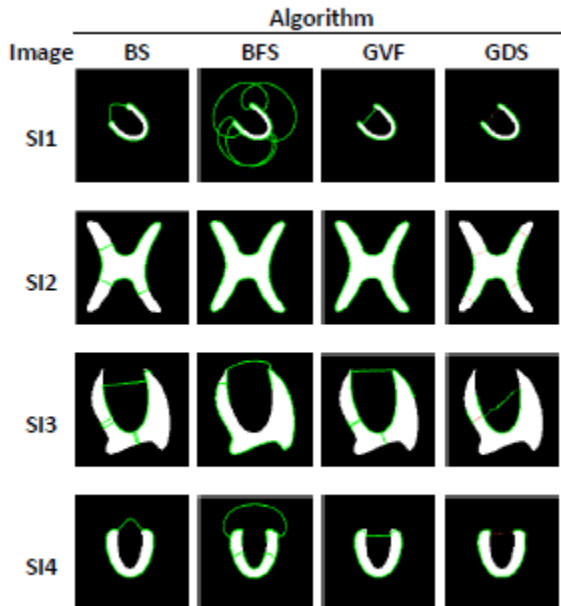


Figure 2.1: H and U simulated shapes and their detected contours with Basis Snake (BS), Balloon Forced Snake (BFS), Gradient Vector Flow (GVF) and Greedy Snake (GDS) algorithms [1].

the fact that organs have smooth surfaces with no sharp edges. Requiring algorithms to yield smooth contour curvatures may improve the results. However, if a constraint on contours from prior knowledge is too strong, solutions will be heavily biased toward prior knowledge and in the extreme can be even flatly wrong. A probabilistic approach to shape analysis, as pursued in this thesis, offers in principle an effective solution by accounting for the degree of uncertainty in prior knowledge. In this thesis, prior knowledge has been incorporated into probabilistic shape determinations by considering spatial relationships between the closest neighbor landmarks along a shape contour via Markov chains and Hidden Markov Models.

2.3 Shape Quantification

In addition to contour detection, another major problem in shape analysis is effectively summarizing complex shape features. The most simplistic summary is using mean and standard deviation, i.e. variance, of contours. While this provides information about global shape features, local variations in shapes are averaged out. Although there are many trivial solutions to measure local shape features, such as computing mean and standard deviation within a patch that slides across the image, the analysis of sliding patches can quickly become overwhelming because of the high dimensional data. A popular method for dimension reduction, while maintaining most of the information, is Principal Component Analysis (PCA) [4]. PCA is a statistical procedure to bring out strong patterns in a multidimensional data, called the principal components. Applied to shape analysis, the largest principal

components will contain most important characteristics whereas smaller components can be ignored, resulting overall in a reduction of data dimension. A problem of PCA is that the dimension reduction is accomplished by transforming correlated input variables into a set of only linear uncorrelated output variables while potentially nonlinear correlations are ignored. The restriction to linearity might miss important information about shapes and also could lead to a bias [4]. To relax the linearity restriction, Fractal analysis has been proposed for characterizing shapes. Fractal analysis evaluates the characteristics of shapes in terms of complex patterns that are self-similar across different scales, the so called fractals [5]. However, Fractal analysis has various methodological issues. In particular, as Fractals are generally derived empirically, a generalization is often limited. Furthermore, a fundamental limitation of both PCA and Fractals in the context of probabilistic shape is that they are both deterministic formalism providing no means to determine the degree of confidence in the shape feature extractions.

2.4 Probabilistic Shape Modeling

To summarize, conventional Snakes algorithms have limitations for extracting contours. In addition, popular methods such as PCA and Fractals can be ineffective for quantifying shapes. In this thesis, a novel probabilistic shape model is used for contour extraction that has been developed by Le.T and Schuff.N [1]. Figure 2.2 demonstrates that simulations for the probabilistic method outperforms Snakes, as illustrated in figure 2.1. However, tests of the probabilistic shape extraction method on experimental data has been limited so far. A major focus of this thesis is to adapt the probabilistic method for extracting shapes of the tongue during vowel generation.

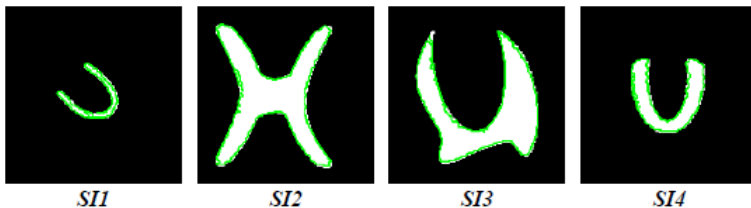


Figure 2.2: H and U simulated shapes and their detected contours using the probabilistic shape model [1]

Chapter 3

Theory

In this section, the principal elements of the novel probabilistic shape analysis approach will be presented.

3.1 Sparse Image Representation

Image feature extraction is typically performed by sparse representation of images in terms of selected basis functions where the function coefficients contain most of the image information, e.g. the location of sharp boundaries. Trigonometric basis functions such as cos and sin, which are the basis of Fourier transform, are widely used for this purpose. However, trigonometric functions are not spatially selective and therefore are not very effective in representing sharp boundaries [13]. In contrast to trigonometric basis functions, Wavelet basis functions offer greater spatial selectivity. Wavelets are widely being used in imaging for multiscale feature extraction. However, neither trigonometric nor Wavelet basis functions provide angular information, which is important for curved boundaries. As a generalization of Wavelets, more recently, Curvelet basis functions have been introduced, which provide angular as well as intensity information [14]. For the purpose of probabilistic shape representations, this thesis used Curvelets.

3.1.1 Curvelet Transformation

Curvelets are designed to provide directionality representation of shape boundaries in images. The Curvelet transformation has been developed by Candes and Donoho in 2000 [14] as a generalization of Wavelet transformation that provides directionality representation of points in an image. In 2006, a new version of Curvelet transformation, named Fast Digital Curvelet Transformation, has been introduced to make Curvelet transformations computationally tractable [3]. Curvelet basis functions are scalable and multidirectional. Furthermore, Curvelet coefficients obey a Gaussian distribution [15]. In order to perform Curvelet transformation, first a 2D Fourier transform of the image is taken and represented in radial coordinates. Afterwards, the 2D frequency domain is divided into parabolic wedges which results in partitioning the Fourier plane in radial coordinate and angular divisions, as illustrated in figure 3.1.

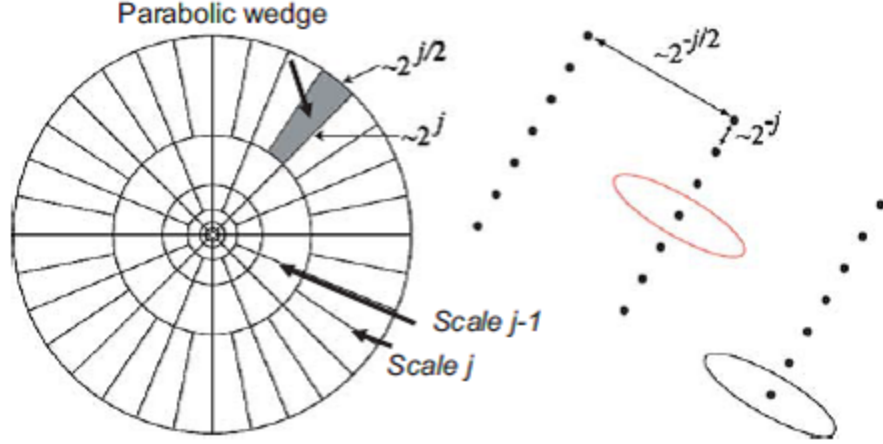


Figure 3.1: Curvelets in Fourier frequency (left) and spatial domain (right) [3].

The multi-size circles indicate multiscale image decomposition and the angular wedges correspond to directionality and orientation. Thus, a particular wedge is defined by a certain scale and a given angle. Figure 3.1 shows the Curvelet coefficients in Cartesian coordinates as well.

Here is a brief description of basic principles of Curvelet transformation. Let $W(r)$, $r \in (1/2, 2)$, and $V(t)$, $t \in (-1, 1)$, be a pair of smooth and non-negative real-valued functions. $W(r)$, the radial window, and $V(t)$, angular window satisfy the admissibility conditions as follows,

$$\sum_{j=-\infty}^{\infty} W^2(2^j r) = 1; r \in \left(\frac{3}{4}, \frac{3}{2}\right) \quad (3.1)$$

$$\sum_{l=-\infty}^{\infty} V^2(t - l) = 1; t \in \left(-\frac{1}{2}, 1\right) \quad (3.2)$$

For each $j \geq 0$ as a scale factor, the window U_j in Fourier domain is defined as,

$$U_j(r, \theta) = 2^{-\frac{3j}{4}} W(2^{-j} r) V\left(\frac{2^{\frac{j}{2}} \theta}{2\pi}\right) \quad (3.3)$$

where (r, θ) denotes the polar coordinate. A Curvelet function ϕ_{jlk} is described by three parameters: a scale 2^{-j} , a direction index l and a position k , defined as,

$$\phi_{jlk}(x) = \pi(R_{\theta_{jl}}(x - x_k^{jl})) \quad (3.4)$$

where $\phi_j(x) = U_j(0, 0)$ and the Curvelet at scale 2^{-j} is $\theta_{jl} = 2\pi \times 2^{-|\frac{j}{2}|} \times l$, $l \geq 0$, $0 \leq \theta_l \leq 2\pi$. Curvelet coefficients are computed using the inner product of the image and the curvelet transform,

$$c_{jlk}(x) = \langle f(x), \phi_{jlk} \rangle \quad (3.5)$$

The image therefore can be represented as a Curvelet series,

$$f(x) = \sum_{jlk} c_{jlk} \phi_{jlk} \quad (3.6)$$

3.2 Markov Chain and Hidden Markov Model

Prior knowledge of smoothness of organs incorporated into shape modeling can improve results. Smoothness can be imposed on contours by taking into consideration that nearest neighbor landmarks are spatially related. An effective model for neighbor relationships along a contour is a Markov Chain model, as explained further below. In addition, Hidden Markov Models will be employed to characterize variations in Markov chain sequences along contours.

3.2.1 Markov Chain Model

A Markov chain model, best known from time series analysis, is a collection of random variables, generated by a random process in which future states conditionally depend on the present and past states [16]. In the context of image contours, a Markov chain model can be envisioned to describe the angular distribution at a new landmark position as conditionally dependent on the neighboring landmark angular distributions. As a result, a large angular deviation, such as a U-turn, will be unlikely in a new landmark if the angular distribution of neighboring landmarks were narrow. Next, a hidden Markov model will be used to characterize the random process that generated variations in Markov chain sets.

3.2.2 Hidden Markov Model (HMM)

HMM is a statistical approach for modeling of symbolic sequences, i.e. variations in Markov chain sets. In imaging, HMM has widely been used in contour completion analysis and object tracking due to its ability of working as a generative model of contour progression [17, 18, 19]. In this thesis, HMM is exploited to effectively extract angular distributions along contours that ultimately lead to the quantification of probabilistic shapes.

To employ HMM for angular distributions along contours, consider a contour S of N landmarks, $S = \{s_1, s_2, \dots, s_N\}$, where s_i is the i_{th} landmark angle. Each $s_i \in S$, is determined based on a set of D different angles, which are defined by the Curvelet transformation scaling factor j (see paragraph on Curvelets above). Typically, $D = 8$ yields sufficient angular resolution for a MRI of size 256×256 . The $D = 8$ angular resolution is derived using chain coding method as shown in figure 3.2.

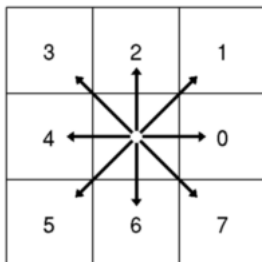


Figure 3.2: Eight connected chain coding to achieve 8-angular resolution [1].

Now, a turning angle between a pair of neighboring landmarks on the contour can be defined as differences between the 8 possible angles at each landmark. Thus, the number of possible

turning angles between two landmarks is 16. Let $O = \{o_1, o_2, \dots, o_{16}\}$, be the set of possible turning angles between two landmarks. HMM models S using a sequence of hidden states Q , $Q = \{h_1, h_2, \dots, h_N\}$, where h_i is the selected hidden state of the i_{th} landmark that generated the angle distribution of s_i in S . Each h_i of Q comes from a predefined hidden state space H , $H = \{H_1, H_2, \dots, H_M\}$ where M is the number of hidden states of HMM. Determining M is specific and hard problem. In this thesis, M is set to 8 to represent 16 different observations based on 8 hidden states. In HMM, choosing the hidden state for the i_{th} observation is based on the probabilities of transition between hidden states and the probabilities of producing the observation by the states. Accordingly, a HMM consists of:

1. Sets of hidden states, H , and observations, O ,
2. The transition matrix A with elements a_{ij} where $i, j = 1, \dots, M$, is the probability of transition from state H_i to state H_j ,
3. The observation probability matrix $B = \{b_{ki}\}$ where b_{ki} is the probability of the observation O_i given the state H_k ,
4. The initial distribution of hidden states, p

Hence, an HMM model l is a tuple of the three parameters, $l = (A, B, p)$, describing the probabilities of transition between hidden states, the probabilities of observations given the state, and the state prior probabilities respectively. Given a sequence S , the objective function of l is:

$$\lambda(S) = \pi(h_1) \times \prod_{i=1}^N P(h_i|h_{i-1}) \times P(s_i|h_i) \rightarrow \max \quad (3.7)$$

Where $P(h_i|h_j) = a_{ij}$ and $P(s_i|h_i) = b_{ii}$. The HMM l can perform following routines:

1. Evaluating: to compute the probability of generating S ,
2. Decoding: to determine the most probable state sequence that produces S ,
3. Training: to estimate the model parameters A, B, p to maximize the objective function $l(S)$.

In this thesis, for contour detection a probabilistic method has been used to select contour among different possible landmark candidates, i.e. Bayesian model, in which HMM is first trained to approximate contour progressions in a contour subset. The decoding functionality the trained HMM is then used to produce the sequence of hidden state vectors of each given sequence, which is used as contour progression description and applied in sequence complexity computation.

3.2.3 Hidden Semi Markov Model (HSMM)

A traditional HMM has the drawback that hidden states are assumed to follow a random Markov process [20]. A Markov process is a stochastic model with the property that hidden state changes only depend on the current state and are not repeated by other hidden states.

In contour progression problems, however, a state change might occur again from other hidden states due to contour bending trends. Selecting an appropriate HMM is therefore essential for model accuracy. Among possible HMM models, the recently developed HSMM is chosen because it allows repetition of hidden states and has stability and fast convergence [20]. Consider $P = \{P_1, P_2, \dots, P_M\}$ where $P_i = \{p_{i1}, p_{i2}, \dots, p_{iZ}\}$ and p_{ij} is the probability that hidden state H_i to be repeated j times. Z , termed sojourn, is the maximum length of hidden states that can be repeated.

An HSMM model λ is a tuple of (A, B, p, P) , where A, B , and p are identical to those of HMM; P is sojourn probability distributions of hidden states. Similar to HMM, HSMM approximates the symbol sequence using a sequence of hidden states that generate a sequence of observations. To determine the hidden state to be selected at landmark i , HSMM produces a vector of hidden state probabilities v_i at the i_{th} contour location s_i , resulting in a sequence of hidden state vectors V , $V = \{v_1, v_2, \dots, v_N\}$, where $v_i = \{v_{ki}\}; k = 1, \dots, M$ and v_{ki} is the probability of observing s_i within the hidden state space H_k . Given a contour S , HSMM computes V using a HMM decode routine. The hidden state vector sequence V describes the probabilistic bending variation of contour S . The probabilistic bending variation at each landmark along S is then used to summarize probabilistic shape information in terms of the E and SC of the bending variations of S .

3.2.4 HSMM training

Given a set $U = \{S_i\}; i = 1, \dots, n$ of contour sequences, a HSMM model is then trained on its attributes A, B, p and P that maximize the objective function in equation (3.7) for every sequence S_i of U . Baum-Welch [21], a popular HMM training algorithm based on Expectation Maximization, was used in this thesis. For initialization, the mean and variance of each model parameter are estimated based on the values of the contour sequences U . The gradient descent learning law is further applied during Expectation Maximization to prevent the training process from yielding oscillatory solutions [1].

3.3 Information Theoretic Measures

Since the probabilistic approach for contour detection incorporates uncertainty of the turning angle variation along contours, information theoretic measures, such as the E and the SC, can be applied to quantify uncertainty in contour variations that lead to a characterization of the corresponding probabilistic shapes.

Information theory is a broad field of Mathematics, beginning with Claude Shannons seminal work in 1948 to quantify information of noisy signals [22]. Today, information theory has broad applications in a wide spectrum of fields from management to biology. With regard to quantifying probabilistic shapes in this thesis, established measures such as the entropy [22], the statistical complexity [6], and the Jensen-Shannon divergence [23] are used to quantify respectively overall shape curvature, curvature variation, and similarity between distributions.

3.3.1 Entropy

Given random values $x \in s$, i.e. image intensities, the entropy is the average uncertainty or - in other words - the degree of surprise associated with observing x in a set of random variables, s . The entropy is defined as:

$$E = - \sum_{x \in s} P(x) \log(P(x)) \quad (3.8)$$

Here, $P(x)$ is the probability of $x \in s$ occurring in any of possible states s . Possible states of a binary random system of zero and one are for example $s = \{[0, 0], [0, 1], [1, 0], [1, 1]\}$ for states of size = 2. The E is always non negative and $0 \log 0$ for $P(x) = 0$ is zero by definition. Obviously, the entropy is a measure of information since a surprising observation carries more information than observations that occur more frequently. In this thesis, the entropy is used to quantify the overall angular distribution of probabilistic shape curvatures.

3.3.2 Statistical Complexity

Statistical Complexity quantifies the complexity of a random system. Various definitions for SC have been introduced. In this thesis the high-dimensional SC has been used which was introduced by Young.K and Schuff.N in 2008 for imaging [6]. Let s be a set of states again and x and y random values of s . Then SC is defined as:

$$SC = - \sum_s \sum_{x,y \in s} P(x|y) \sum_{x,y \in s} \log(P(x|y)) \quad (3.9)$$

$P(x|y)$ is the probability of observing x conditionally to having observed y . The sums run across all observations x and y and all possible states s . SC can be interpreted as the difficulty to discover information in a stochastic sequence. Obviously, information is easy to discover from sequences that are strictly periodic or completely random (i.e. zero information), while retrieving information from any sequence in between these extremes is complex. In this thesis, SC is used to quantify the variability in the angular distributions of probabilistic shape curvatures.

3.3.3 Jensen-Shannon Divergence

Lastly, the Jensen-Shannon Divergence (JSD) is used to determine similarity between probability distributions, i.e. the similarity between the distributions of hidden states for two neighboring landmarks on a contour. Obviously, it is reasonable to assume that the angular variation between two neighboring landmarks is small if the two landmarks are associated with similar hidden states distributions. In contrast, the angular variations between the landmarks could be large if their corresponding hidden states distribution differ significantly. JSD quantifies how much two probability distribution differ. JSD is defined as:

$$JSD(P, Q) = E\left(\frac{P + Q}{2}\right) - \frac{1}{2}(E(P) + E(Q)) \quad (3.10)$$

Here, $E(P)$ and $E(Q)$ are the entropies of distribution P and Q , respectively. In this thesis, JSD is used to derive the turning angle probability between two landmarks given the uncertainty of the angular distributions at each landmark.

Chapter 4

Method

4.1 Subjects and Study Protocol

Five healthy subjects [1 woman, 4 men, age range 24-58] were recruited for this study. The study was approved by the Institutional Review Board of the UCSF (University of California, San Francisco) and all subjects provided written informed consent. All subjects spoke English but were different native speakers. The subjects included 1 German speaker, 1 French, 1 Chinese mandarin and 2 Persian speakers. All subjects were asked to sequentially pronounce the vowels [u:], [i:], [a:], [ae:], [e:], [o:], each for approximately 7 seconds, while lying in an MRI machine and having a fast MRI scan of the tongue.

4.2 MRI Acquisition

2D MRI scans were obtained with high temporal, spatial image resolution and good soft tissue contrast using a MRI Fast Low Angle Shot(FLASH) sequence that was introduced by A. Haase et al.[2]. FLASH is a gradient echo based sequence technique that uses very low flip angle in order to obtain a sufficiently high yield of the MRI signal while avoiding long waiting time between successive experiments for signal recovery. The FLASH sequence was setup for optimal contrast to noise within a short acquisition time without losing spatial resolution. Since the flip angle is very short, low rf power is required. Taking the advantage of the FLASH sequence, a movie of tongue movement during speech is possible [24].

The MR images of the tongue were acquired on a standard clinical 3.0 Tesla MRI Siemens Skyra system with a 32-channel head coil. For each vowel, seven image frames of the 2D mid sagittal slice of the tongue were acquired from each subject. Other relevant imaging parameters were: 1.5mm in-plane resolution, 10mm slice thickness, 36.7 ms repetition time, 1.36ms gradient echo time, and 5 degree flip angle.

The total scan time for 42 image frames (6 vowels and 7 frames per vowel) was approximately 10 minutes for each subject.

4.3 Preprocessing

Head MR raw images which covered brain and mouth were smoothed with a spatial median filter in order to reduce noise. The area around the tongue was cropped using a rectangular and anatomically registered mask.

4.4 Bayesian Contour Extraction

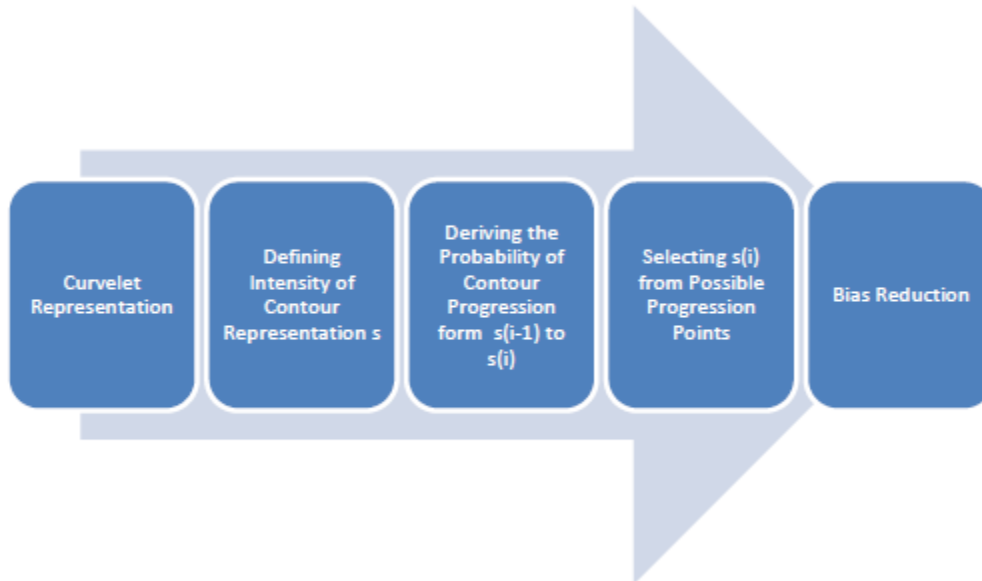


Figure 4.1: Flow chart of Bayesian Contour extraction modeling.

In the following sections, the extraction of tongue surface contours using probabilistic Bayesian shape model is derived.

4.4.1 Curvelet Representation

Next, the contour extraction model is derived from Curvelet representation of images as defined in equation (3.6). The determination of scale j of Curvelets is problem specific. For the purpose of probabilistic shape modeling, the scale $j = 8$ was used, although other scales could be more effective solutions to certain problems.

Let c_k be the maximum curvelet coefficient and θ_k the corresponding direction at the location k in the curvelet representation of the image, defining a landmark point in the landscape of all coefficients and directions. Since the curvelet coefficients surrounding a landmark point follow a normal distribution $N(k, c_k)$ [19], the conditional probability of a neighbor k' given k is defined according to:

$$P(k'|k) = \frac{1}{c_k \sqrt{2\pi}} \exp\left(-\frac{|k' - k|}{2c_k^2}\right) \quad (4.1)$$

The coefficient distribution at k' can be approximated according to:

$$P_{k'} = \frac{1}{n} \sum_{k'=1}^n P(k'|k) \quad (4.2)$$

$$\sigma_{k'} = \sum_{k'} P(k', k) \times |k' - k| \quad (4.3)$$

Here, $p_{k'}$ is the prior probability of the coefficient probability distribution at k' and $\sigma_{k'}$ is the standard deviation of the approximation. The better estimation of $\sigma_{k'}, \sigma_{k'}^*$ is defined as:

$$\sigma_{k'}^* = \min\{c_{k'}, \sigma_{k'}\} \quad (4.4)$$

4.4.2 Defining Intensity of Contour Representation

Next, the extraction of contour representations in the curvelet representation of the image is described.

Let S be a contour represented by the k landmark points, $s_i, i = 1, \dots, k; S = (s_1, s_2, \dots, s_k)$. The intensity of S is defined according to:

$$D(S) = \sum_{s_i} P(s_i|S^{i-1}) \times c_i \quad (4.5)$$

Where $P(s_i|S^{i-1})$ is the probability of the contour S^{i-1} progressing to s_i and c_i is the corresponding Curvelet coefficient. A first order Markov chain model is then applied to derive the contour progression. The first order Markov chain model is defined according to:

$$P(s_i|S^{i-1}) = P(s_i|s_{i-1}) \times P(S^{i-1}) \quad (4.6)$$

With,

$$P(s_i|s_{i-1}) = P(s_i|s_{i-1}, \theta_i) \times P(\theta_i|s_{i-1}, \theta_{i-1}) \quad (4.7)$$

4.4.3 Deriving the probability of contour progression

The first term of equation (4.7) at lhs is the probability of progression to s_i , given s_{i-1} and the selected progression angle θ_i (see further below for the selection probability). The second term on the rhs describes the probability of switching direction from θ_{i-1} to θ_i . Given the probability of switching direction, the probable angle for the contour progression from s_{i-1} to s_i will then depend on the coefficients c_{i-1} and c_i according to:

$$P_{\theta(i-1)}^i = \exp - \frac{|c_{i-1} - c_i|^2}{2 \times (c_i)^2} \quad (4.8)$$

4.4.4 Selecting Best Progression Point

In general, several points, can be candidates for progression. Thus, a method needs to be developed for guiding the selection given the data. Here, it is postulated that the best selection

of a candidate is the one which provides maximum gain in information for the progression. This is equivalent to minimizing the mutual information between the distributions of possible points. In detail, given two data points, s_i and s_j , and their corresponding distributions, D_i and D_j , the mutual information between the distributions is:

$$I_M(D_i, D_j) = \sum_{d_{ik} \in D_i} \sum_{d_{jl} \in D_j} P(d_{ik}, d_{jl}) \log \left(\frac{P(d_{ik}, d_{jl})}{P(d_{ik})P(d_{jl})} \right) \quad (4.9)$$

Here, d_{ik} is the conditional probability of point k given the point i . Therefore, a solution for the contour evolution where information is maximized is needed. To find the solution that maximizes information, $I_M(D_i, D_j)$ is first normalized according to equation (4.10), before integrating over all possible solutions to find the one yielding maximum information gain.

$$I_N(D_i, D_j) = \frac{I_M(D_i, D_j)}{\max_{k,l} \{I_M(D_k, D_l)\}} \quad (4.10)$$

The contour S^* represents a feature boundary in the image if and only if it holds the criterion in equation (4.11), that leads to the model of contour detection algorithm. $I_N(s_{i-1}, s_i)$, the normalized mutual information is computed using the coefficient distributions at s_i and s_{i-1} , according to equation (4.10).

$$D(S^*) = \max_i \{D(S^i)\} \quad (4.11)$$

$$D(S^i) = \max_{s_{i-1}} \{B(s_{i-1}, s_i) \times P(s_i | S^{i-1}) \times c_i + D(S^{i-1})\} \quad (4.12)$$

$$B(s_{i-1}, s_i) = \frac{1}{I_N(s_{i-1}, s_i)} \quad (4.13)$$

To summarize, $D(S^*)$ is the contour intensity of the probabilistic model S^* . $D(S^i)$ is the intensity of contour length i .

4.4.5 Bias Reduction

In general, $D(S^*)$ will be biased toward the initial point selection. To reduce bias, multiple contours using random selection of the initial points are computed. A search for a contour using the model in equation (4.9) can be done using a dynamic programming algorithm in combination with multiple initial point selection [1]. This yields multiple contours which describe slightly different as well as overlapping image features. A post analysis on the detected contours is needed to identify the key features in of the image. This is accomplished as follows: Let C^* be the set of common landmarks in the detected contours, $C^* = \cap S_i$, $i = 1, \dots, m$, where m is the number of detected contours. Let $F(p)$ be the frequency function defined on C^* as in equation (4.14).

$$F(p) = \frac{1}{m} \sum_{i=1}^m I(p \in S_i) \quad (4.14)$$

Where

$$I(x) = \begin{cases} 1 & ; x=\text{true} \\ 0 & ; x=\text{false} \end{cases} \quad (4.15)$$

Each detected contour will be assigned a rank index based on how it covers the common landmark set, defined as in

$$R(S) = \sum_{k \in S} F(k) \times p_k \times c_k \quad (4.16)$$

The contour S^* having the highest rank value will be selected as the first key feature of the image. For additional key features, we define:

$$M^k = \cup_{i=1}^k S^i \quad (4.17)$$

The similarity measurement of contours is determined based on the distributions of contour conditional probabilities, according to:

$$Score(S) = \frac{R(M^k) - R(S)}{R(M^k)} \times \frac{I_M(S, M^k)}{I_M(M^k, M^k)} \quad (4.18)$$

where M^k is the set of points in k selected features.

In these approaches, $[p_1, p_2]$, the overlap between a contour S and the set of selected contours is computed using the contour overlapping density. The "new" property of a contour S is determined based on the information gained by adding S to the selected contour set. A contour S will be the $(k + 1)^{th}$ selected feature if and only if:

$$Score(S') = \min_{i=1, \dots, m} \{S^i\} \quad (4.19)$$

For selecting a contour likelihood based approach is used in this method; each candidate contour will be assigned a log-likelihood index based on how likely it is regarding the HMM of the detected contours in the image. Maximization of the likelihood will provide the best contour solution, according to:

$$Score(S) = \frac{R(M^k \cap S)}{R(M^k)} \times \frac{I_M(S, M^k)}{I_M(M^k, M^k)} \quad (4.20)$$

The first term, on the lhs, indicates how much S overlaps with the selected contours; the second term on rhs indicates how similar S is regarding the selected contour set. For potential candidate S , both the terms should be minimized.

4.5 Feature Extraction

Based on the probability model described above, we have a contour containing many landmark points and directionality information including a set of 16 different turning angles from the Curvelet transformation in addition to position knowledge for each landmark. To impose smoothness on the contours curvature, given prior knowledge that the imaged physical objects are smooth, the probability of turning angles between neighboring landmark points can be computed using a Markov chain model (as described in previous section (3.2)). Furthermore, the probability distributions of 8 hidden states can be derived from aggregated contours. In this study, the aggregation includes 42 contours per subject from all 7 images frames per vowel and 6 vowels per subject.

Given the distribution of hidden states, the turning angle between a pair of neighboring landmark points on a contour is then computed as difference between the pair of landmark angles weighted by the JSD of the corresponding hidden states to enforce smoothness, as expressed in equation (4.21). Again, the idea is that similar distributions of hidden states between neighboring landmarks, yielding JSD values near zero, are probably generating similar angular distributions and therefore the occurrence of large turning angles between such landmarks is penalized. In contrast, for vastly dissimilar distributions of hidden states between neighboring landmarks, yielding JSD values near unity, the occurrence of large angular differences is expected.

$$D_{ij} = |\theta_i - \theta_j| \cdot JSD(P_i, P_j) \quad (4.21)$$

The sequence of D_{ij} values from a contour reflects the curvature of that contour. To effectively summarize variations in contour curvatures, the D_{ij} values are then assembled in a co-occurrence matrix X where each D_{ij} value is plotted against any other D_{ij} value and the sum of all occurrences is normalized to one to express X in terms of probability. Given that D_{ij} can take 16 values in this study based on a Curvet angular resolution of 8, the X matrix in this study is of size 16×16 .

4.6 Quantification of Features

The X , 16×16 matrix, is basically a two dimension histogram of turning angle distributions of a contour, capturing the curvature of the contour. The E and the SC of X are then computed according to equations 3.8 and 3.9, to quantify curvature. Specifically, the E measures the degree of turning angle distributions that determines the overall curvature features of a contour. For a curvature with largely flat features, the E will be small, because the distribution of turning angles will be narrow. In contrast, for a curvature with mainly round features the E will be large, because the distribution of turning angles will be wide. SC measures the degree of variability in turning angle distributions. For a curvature, whether flat or round, but with many local varying features, SC will be large. For a curvature with locally more uniform features, SC will be small. Each E or SC alone or both together can be used to classify shapes. In this thesis, the various shapes of the tongue when pronouncing different vowels is measured using E, SC, as well as E and SC together.

4.7 Computational language method

All algorithms have been coded in Matlab.

4.8 Statistics

The sensitivity of novel approach to capture characteristic tongue shapes during vowel generation was tested across 210 shape models from contours of the tongue of 5 subject, 6 vowels, and 7 MRI frames. First, it was tested whether the novel probabilistic shape method can capture variations in tongue shapes when pronouncing vowels, compared to shape variations

of the tongue at rest, i.e. variations across repeated measurements. This was accomplished by separately modeling each shape metric, i.e. E or SC, as a function of vowel as well as MRI scan number. To further consider variations across subjects, the design was extended to a mixed effects model with vowels as fixed effect and variations between subjects as random effect. Second, it was tested whether the novel probabilistic shape method can further capture a characteristic tongue shape of each vowel across subjects. This was accomplished by contrasting the shape variations between vowels in a mixed effects model with vowel by frame interactions across subjects. Moreover, in order to explore the benefit of using E and SC together for probabilistic shape characterization, univariate mixed effects models for each metric were expanded to a multivariate one in which SC and E were used simultaneously. This was accomplished using a Monte Carlo sampling library in R using the `MCMCglmm` function.

To determine statistical significant, a bootstrap was used to obtain distributions of the modeling coefficients, and their 95% confidence interval was evaluated to determine statistical significance.

Chapter 5

Initial Test

As initial test of shape method, a recorded movie of hand shapes as shown in figure 5.1 was used. The images provided high contrast and well defined features, i.e. finger positions. The raw images of different hand gestures extracted from the video are shown in below.

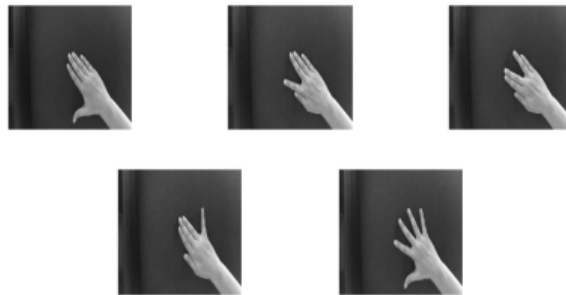


Figure 5.1: Different hand gestures numbering one to five, respectively.

Results of contour extraction from the hand are shown in figure 5.2.



Figure 5.2: The green lines shows extracted contours using the novel probabilistic shape model.

Note, in the second and fourth hand shapes, there are sharp edges that are difficult to detect with the probabilistic method due to the assumption of smoothness and this leads to incomplete contours. Nonetheless, the main features of hand shapes are successfully detected. The

probabilistic algorithm successfully detected hand gestures in 9 frames for first gesture, 10 frames for second gesture, 9 frames for third, 10 frames of fourth gesture and 2 frames for fifth gesture (total 40 frames).

In the scatter plot below, SC is plotted versus E for each hand gesture. Each color corresponds to the specific hand gesture shown in figure 5.1.

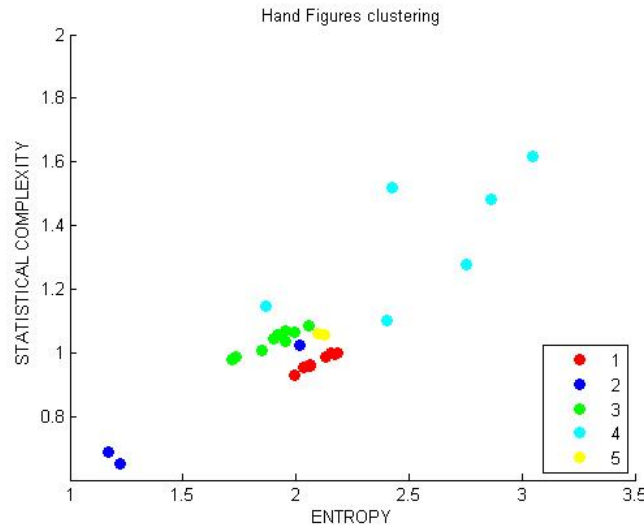


Figure 5.3: Plot of SC versus E for different hand gestures. Colors indicate the various hand gestures shown in figure 5.1. Note, the clustering in SC and E for most hand shapes.

Note, the E and SC are correlated to each other i.e. more E results in more complex data as expected. More E means wider range of angles in landmarks and higher SC means more angle variations between the landmarks. The scatter plot also indicates that some hand gestures can be clearly separated based on E and SC, such as gestures number 1, 3 and 5 in figure 5.2 while others overlap.

Chapter 6

Main Results - Tongue Shapes

Representative raw images from a subject while pronouncing 6 vowels, [u:], [i:], [a:], [ae:], [e:], [o:] respectively are shown in figure 6.1.

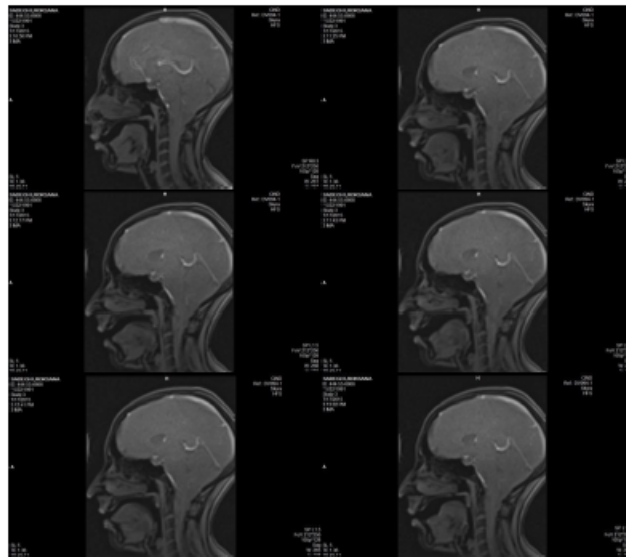


Figure 6.1: Representative MRI data from a subject pronouncing 6 vowels. The images have been acquired with MRI Skyra system with 32 channel head coil and the Flash sequence. The important parameters of the sequence can be found in the images. The images in the first row corresponds to vowels [u:] and [i:], second row [a:] and [ae:] and third row [e:] and [o:], respectively.

As mentioned in method section (4.3), image preprocessing involved cropping the main area around the tongue and also spatially filtering to increase signal to noise ratio. The images below, figure 6.2, illustrate the results from preprocessing of the raw images shown in figure 6.1.

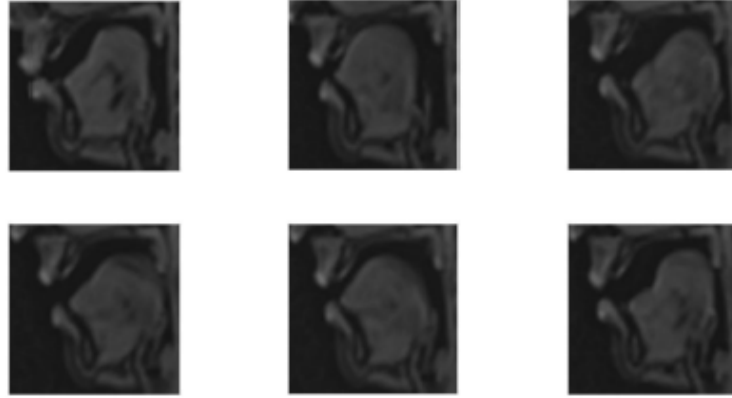


Figure 6.2: Preprocessed images of the same subject as shown in figure 6.1 while pronouncing 6 vowels. The images in the first row corresponds to vowels [u:], [i:] and [a:] and second row [æ:], [e:] and [o:], respectively.

Contours of the tongue shapes for various vowel pronunciations obtained using the novel probabilistic shape method are shown in figure 6.3.

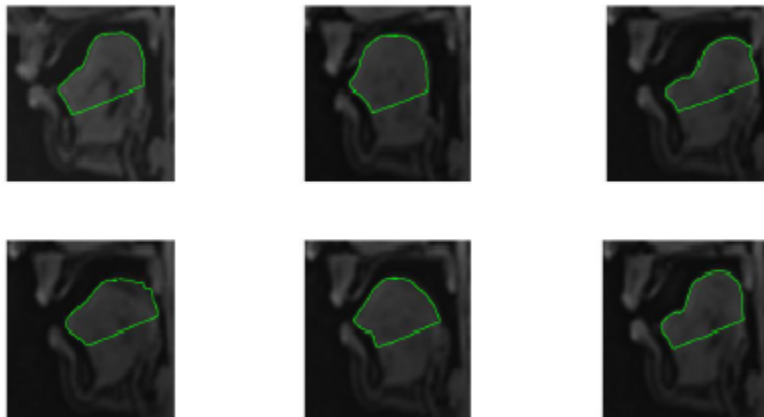


Figure 6.3: Contours extraction of the same subject pronouncing different vowels.

To illustrate between subject variability in tongue shape, images in figure 6.4 shows data from different subjects pronouncing vowel [i:]. As one can see, different subjects have different shape of tongue for pronouncing same vowel.

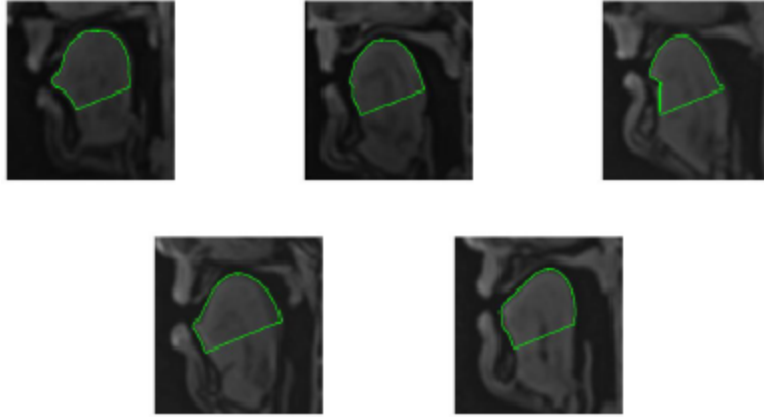
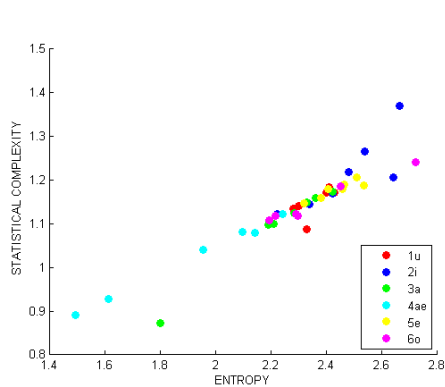


Figure 6.4: Different subjects pronouncing [i:] under the MR System.

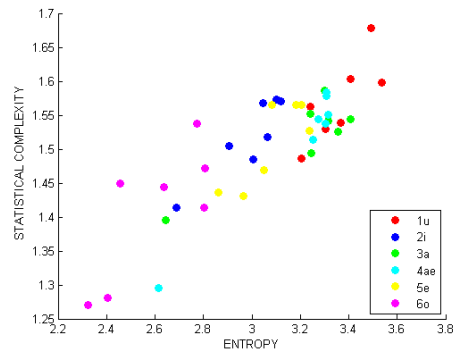
The scatter plots in figure 6.5 depict SC versus E of tongue shapes when pronouncing different vowels for each of the subjects. The colors indicate the different vowel.

Note, in all subjects the E and SC are correlated to each other i.e. more E results in more complex data as expected. More E means wider range of angles in landmarks and higher SC means more angle variations between the landmarks. The plots show clustering of tongue shapes for vowels in some subjects, although there is variability between subjects.

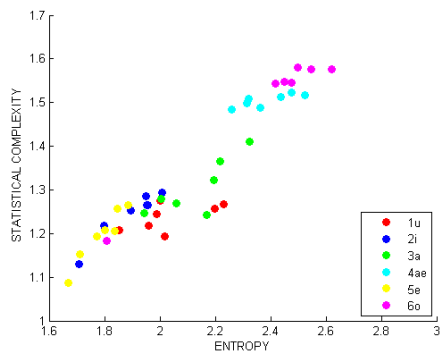
The first test was to determine whether any vowel explains variations in either E or SC significantly better than repeated scans. For both E and SC, the effect of vowels on variations was markedly strong (p-value = 0.0540 and 0.0319 respectively) than the effect of repeated scan, demonstrating that the novel method can capture tongue shapes associated with a particular vowel. The second test was to determine whether variations in either (E, SC) or (E and SC together) vowels are associated with individual vowels across subjects. Table 6.1 provides the summary of p-values from univariate models. For E, consistent variations at the 95% confidence level were associated with vowels [u:], [ae:] and [o:] (p-value < 0.05). For SC, consistent variations at the 95% confidence level were associated with vowels [u:], [ae:], [o:] and [a:] (p-value < 0.05). For E and SC used together, consistent variations were associated with vowels [a:], [e:], [i:], and [u:] with (p-value \leq 0.05).



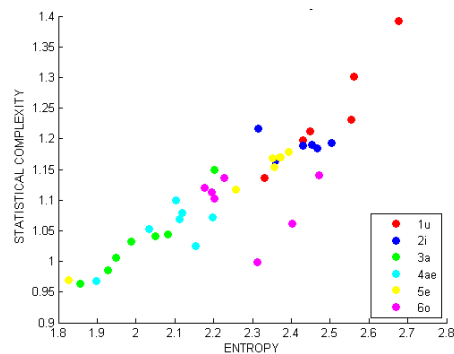
(a) Subject A. Note, the light blue and blue has been well clustered.



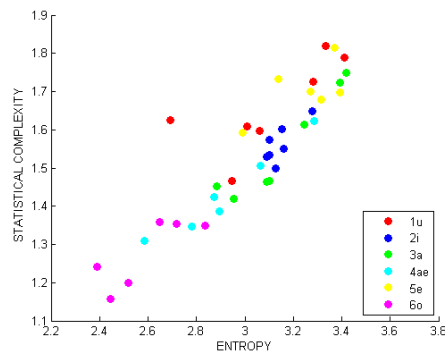
(b) Subject B. In contrast to previous subject, almost all vowels has been clustered except green.



(c) Subject C. In this subject, the blue and yellow are not distinguishable but the green, red, light blue and purple are perfectly clustered.



(d) Subject D. Similarly, the plot of Entropy vs. SC has clustered the different vowels.



(e) Subject F. In this subject, the purple and blue is clustered but the other vowels are not distinguishable.

Figure 6.5: Plot of SC versus E in 5 subjects

Fixed Effects	p-values of E model	p-values of SC model
Intercept	< 0.001*	< 0.001*
[i:]	0.167	0.373
[a:]	0.536	0.019*
[ae:]	0.016*	0.047*
[e:]	0.091	0.284
[o:]	< 0.001*	< 0.001*
Frame-2	0.607	0.741
Frame-3	0.371	0.883
Frame-4	0.297	0.505
Frame-5	0.254	0.679
Frame-6	0.576	0.957
Frame-7	0.267	0.581

Table 6.1: **Univariate analysis of E and SC separately.** This table contains p-values of variations from different vowels as well as different frames from univariate mixed effect model considering E and SC. Note, the one with * significantly detected with the corresponding model

Fixed Effects	p-values of E and SC model
Intercept	0.046*
[ae:]	0.220
[e:]	0.038*
[i:]	0.040*
[o:]	0.196
[u:]	0.050*
Frame-2	0.994
Frame-3	0.132
Frame-4	0.942
Frame-5	0.530
Frame-6	0.402
Frame-7	0.692

Table 6.2: **Multivariate analysis of E and SC together.** This table contains p-values of variations from different vowels as well as different frames from multivariate mixed model considering both E and SC. Note, the one with * significantly detected with the model

Chapter 7

Discussion and Conclusion

A novel model for contour extraction in MRI was tested that utilizes a probabilistic formalism to incorporate uncertainty of shape features. In addition, measures anchored in information theory were used to effectively summarize probabilistic shape features.

The method was initially tested on high contrast images of well-defined hand gestures, demonstrating its ability to capture the characteristic of several gestures. Values E and SC of gestures #2 and #4 in figure 5.2 are different from other gestures because the contour stops half way at the outside hand border, whereas for the other gestures the contours continue. However, this does not explain the large difference in E and SC between #2 and #4. The higher E and SC values of #4 relative to #2 can be explained by the large contour variability around the thumb, index, middle and ring finger in #4. Despite #2, the contour variability is mainly confined to middle and ring finger. By the same token, the explanation for the slightly larger SC value of #3 relative to #1 is the V shaped interruption of the finger contour in #3 that is absent by the closed finger in #1. Since the spread of all fingers makes a V shaped interruption appear more regular again, the SC value of #2 values decreases and falls in the middle between #1 and #3. Taking together, initial tests show that different hand gestures are captured using E and SC.

The method was then tested on tongue shapes when pronouncing vowels [u:], [i:], [a:], [ae:], [e:] and [o:]. The results indicate that the method is able to capture characteristic tongue shapes for all vowels across subjects. In particular, the variations in shape were significantly larger than variations in repeated MRI scans, demonstrating the sensitivity of the approach to detected shapes. Furthermore, it was possible to extract consistent shapes across individuals for vowels [u:], [ae:] and [o:] by considering the E of angular distributions along contour. In addition, considering the SC of angular distributions along contour, consistent variations were associated with vowels [u:], [ae:], [o:] and [a:]. Modeling contours by both E and SC also extract consistent shapes across subjects for vowels [a:], [e:], [i:] and [u:], significantly. The reason why a consistent shape in a model was detected across subjects for some vowels but not for others is unclear. One explanation is that individual tongue shapes vary more for some vowels than for others, potentially in accordance with the native language of the subjects. The number of subjects in this thesis was too small to test this possibility with a reasonable level of confidence. Another explanation is that 2D imaging of the tongue midsection is insufficient to capture the complex tongue motion for pronouncing some of the vowels. An extension of the method to 3D data is required to address this issue.

The most important finding of this thesis is that the probabilistic shape approach resulted in a sensitivity detection of tongue shape during vowel pronunciations.

An important methodological innovation in this thesis is that the degree of smoothness of contour curvatures is data-driven using HSMM in conjunction with a Markov chain model. In contrast, most other approaches of shape extraction use ad-hoc models for smoothness which potentially induce bias on smoothness. The findings of this thesis demonstrate that a data-driven approach is effective. However, an extension of HSMM and Markov chain from contours to planes for 3 dimensional data is challenging and requires substantially more work. In addition, an Expectation Maximization algorithm was used to find the best answer from initial guesses based on maximum likelihood, though it remains difficult whether a global maximum solution is always achieved. Other optimization methods may offer more robust results.

The new method is potential of interest to clinical studies of tongue disorders and function, including speech therapy, assessment of tongue surgery and assessment of functionality of the tongue. Beyond the tongue, the novel probabilistic approach has potentially wide clinical applications in almost any medical field that uses imaging. Examples of applications for the importance of contour extraction and shape detection include the delineation of almost any organ, such as the shape of kidneys and liver, the changing shapes of tendons in joints during movement, the tracking of change in structure of beating heart, and the shape of a tumor, specifically in the brain.

In summary, this thesis demonstrated the successful extraction of shape features of both hand gestures and tongue movement using the novel probabilistic shape model. In addition, the probabilistic nature facilitated quantification of the shapes in terms of E and SC. This approach is potentially applicable in many medical fields.

Bibliography

- [1] Thanh Le and Norbert Schuff. A gradient-based probabilistic method for image feature extraction. *Information Technology: New Generations (ITNG), 2014 11th International Conference on*, pages 143 – 148.
- [2] A. Haase, J. Frahm, D. Matthaei, W. Hänicke, and K.-D. Merboldt. FLASH imaging: Rapid NMR imaging using low flip-angle pulses. *Journal of Magnetic Resonance*, 213(2):533–541, 1986.
- [3] Emmanuel Candès, Laurent Demanet, David Donoho, and Lexing Ying. Fast Discrete Curvelet Transforms. *Multiscale Modeling & Simulation*, 5(3):861–899, 2006.
- [4] Hervé Abdi and Lynne J. Williams. Principal component analysis. *Wiley Interdisciplinary Reviews: Computational Statistics*, 2(4):433–459, 2010.
- [5] C C Chen, John S Daponte, and Martin D Fox. Fractal feature analysis and classification in medical imaging. *IEEE transactions on medical imaging*, 8(2):133–42, 1989.
- [6] Karl Young and Norbert Schuff. Measuring structural complexity in brain images. *NeuroImage*, 39(4):1721–1730, 2008.
- [7] Vijay Parthasarathy, Jerry L Prince, Maureen Stone, Emi Z Murano, and Moriel Nessaiwer. Measuring tongue motion from tagged cine-MRI using harmonic phase (HARP) processing. *The Journal of the Acoustical Society of America*, 121(1):491–504, 2007.
- [8] Olov Engwall. Combining MRI, EMA and EPG measurements in a three-dimensional tongue model. *Speech Communication*, 41(2-3):303–329, 2003.
- [9] M. Kass, a. Witkin, and D. Terzopoulos. Snakes: Active contour models. *International Journal of Computer Vision*, 1(4):321–331, 1988.
- [10] Laurent D. Cohen. On active contour models and balloons. *CVGIP: Image Understanding*, 53(2):211–218, 1991.
- [11] Lilian Ji and Hong Yan. Attractable snakes based on the greedy algorithm for contour extraction. *Pattern Recognition*, 35(4):791–806, 2002.
- [12] S. Kichenassamy, a. Kumar, P. Olver, a. Tannenbaum, and a. Yezzi. Gradient flows and geometric active contour models. *Proceedings of IEEE International Conference on Computer Vision*, pages 4–9, 1995.

- [13] Dengsheng Zhang and Guojun Lu. Review of shape representation and description techniques. *Pattern Recognition*, 37(1):1–19, 2004.
- [14] Emmanuel J. Candès and David L. Donoho. Curvelets - A surprisingly effective non-adaptive representation for objects with edges. *Curves and Surfaces*, C(2):1–10, 2000.
- [15] Jianwei Ma and Gerlind Plonka. The curvelet transform. *IEEE Signal Processing Magazine*, 27(2):118–133, 2010.
- [16] Charles M. Grinstead and J. Laurie Snell. Markov Chains. In *Introduction to Probability*, pages 1–66. 2010.
- [17] Jacob Feldman and Manish Singh. Information along contours and object boundaries. *Psychological review*, 112(1):243–252, 2005.
- [18] Wilson S. Geisler and Jeffrey S. Perry. Contour Statistics in Natural Images. *Visual neuroscience*, 26(1):109–121, 2009.
- [19] Yothin Rakvongthai and Soontorn Oraintara. Statistics and dependency analysis of the uniform discrete curvelet coefficients and hidden Markov tree modeling. In *Proceedings - IEEE International Symposium on Circuits and Systems*, pages 525–528, 2009.
- [20] Ming Dong and David He. A segmental hidden semi-Markov model (HSMM)-based diagnostics and prognostics framework and methodology. *Mechanical Systems and Signal Processing*, 21(5):2248–2266, 2007.
- [21] Lloyd R Welch. Hidden Markov Models and the Baum-Welch Algorithm. *IEEE Information Theory Society Newsletter*, 53(4):1,10–13, 2003.
- [22] C E Shannon. The mathematical theory of communication. 1963. *MD computing computers in medical practice*, 14(4):306–17, 1948.
- [23] Centrum Wiskunde. Properties of Classical and Quantum Jensen-Shannon Divergence. pages 1–13, 2009.
- [24] Martin Uecker, Shuo Zhang, Dirk Voit, Alexander Karaus, Klaus Dietmar Merboldt, and Jens Frahm. Real-time MRI at a resolution of 20 ms. *NMR in Biomedicine*, 23(8):986–994, 2010.

Publishing Agreement

It is the policy of the University to encourage the distribution of all theses, dissertations, and manuscripts. Copies of all UCSF theses, dissertations, and manuscripts will be routed to the library via the Graduate Division. The library will make all theses, dissertations, and manuscripts accessible to the public and will preserve these to the best of their abilities, in perpetuity.

Please sign the following statement:

I hereby grant permission to the Graduate Division of the University of California, San Francisco to release copies of my thesis, dissertation, or manuscript to the Campus Library to provide access and preservation, in whole or in part, in perpetuity.

Rokhsana Sadeghi

Author Signature

8/28/2015

Date